Maxwell *et al. Fire Ecology* (2026) 22:91
https://doi.org/10.1186/s42408-026-00498-0

Fire Ecology

RESEARCH

Open Access

Repeat terrestrial laser scanning for documenting and monitoring prescribed fire efficacy

Aaron E. Maxwell[1*], Michael R. Gallagher[2], Samuel R. Stockton[1], Matthew C. Wozniak[1], Brenden E. McNeil[1], Julia A. Defeo[4], Alexis Everland[5] and Nicholas S. Skowronski[3]

Abstract

Background Prescribed fire is an established means to reduce wildfire risk and accomplish silvicultural and cultural objectives via controlled consumption of fuels. Terrestrial laser scanning (TLS) has been demonstrated as a simple and efficient means to quantify fuel and vegetation conditions in terms of three-dimensional forest structure and occupied volume at the plot-scale; however, there is currently a lack of studies that explore a repeat time series of TLS measurements for documenting fire treatment efficacy over time. We used a time-series approach to repeatedly scan 40 monitoring plots six times over a 4-year period (one pre-fire, one post-fire, and yearly scans over a 4-year period) within a burn unit in the New Jersey Pine Barrens, USA. Our TLS analysis evaluates metrics to quantify first-order effects on forest structure and subsequent structural changes and regrowth. Metrics include the percentage of all returns that were not classified as ground, as well as a volume-based, occlusion-adjusted percentage of non-occluded voxels with returns at the plot- and three strata-levels: canopy, tall shrub, and low shrub. We also made comparisons to other commonly used burn severity assessment methods, including the visual field-based composite burn index (CBI), as well as the Sentinel-2 Multispectral Instrument (MSI)-derived normalized difference vegetation index (NDVI) and normalized burn ratio (NBR).

Results The TLS methods were most effective at characterizing changes in the low and tall shrub strata, which are commonly targeted during prescribed fire treatment. Post-fire change metrics were generally correlated with initial metric values and initial change in metric values, especially in the low and tall shrub strata where all Pearson and Spearman correlation coefficients were above 0.400 and as high as 0.955. We also document correlations among the TLS-based metrics and the initial change and rate of post-fire change in NDVI and NBR and the field- and visual-based composite burn index (CBI). Finally, we document that plot-level metrics can be aggregated to characterize entire burn units.

Conclusions Multi-temporal TLS compliments NBR- and CBI-based assessment and improves the quantification of prescribed fire efficacy for reducing the abundance of fuels in the low and tall shrub strata.

Keywords Terrestrial laser scanning, TLS, Prescribed fire, Wildland fire, Fuels

*Correspondence:
Aaron E. Maxwell
Aaron.Maxwell@mail.wvu.edu
Full list of author information is available at the end of the article

Resumen

Antecedentes Las quemas prescriptas representan un método ya establecido para reducir el riesgo de incendios de vegetación y otros objetivos culturales a través del consumo controlado de los combustibles vegetales. El escaneo terrestre con laser (TLS) ha demostrado ser un método simple y eficiente para cuantificar los combustibles vegetales y sus condiciones de manera tridimensional en cuanto a estructura y el volumen ocupado a escala de parcela; sin embargo. Existe hoy una falta de estudios que exploren de manera repetida En series de tiempo Las mediciones mediante TLS para documentar la eficiencia de tratamientos en el tiempo. Usamos una aproximación de series de tiempo para escanear repetidamente 40 parcelas de monitoreo seis veces en un período de cuatro años (una en el pre fuego Una post fuego y escaneos anuales por un período de cuatro años). Dentro de una unidad de quema en el Pinar de Barren. En Nueva Jersey EEUU. Nuestro análisis de TLS evaluó las métricas para cuantificar efectos de primer orden sobre la estructura forestal y los subsecuentes cambios estructurales y el recrecimiento. Estas métricas incluyen el porcentaje de todos los retornos que no fueron clasificados como suelo Como así también una medida del volumen (i.e. *voxeles Que representan una unidad de medida utilizada en la creación de gráficos en 3D*) Que tenían el porcentaje de oclusiones ajustadas para considerar sólo las oclusiones reales a nivel de parcelay de tres niveles de estratos: los doseles Los arbustos altosy arbustos bajos. También hicimos comparaciones con otros métodos de determinación de severidad comúnmente usadosIncluyendo el índice visual compuesto de campo (CBI)Como así también del Instrumento Espectral del Sentinel-2 (MSI) que deriva en el índice de diferencia normalizada de Vegetación (NDVI) y la relación de relación de quema normalizado (NBR).

Resultados Los métodos de TLS fueron los más efectivos para caracterizar cambios en los estratos de arbustos altos y bajos Los cuales son generalmente definidos como un objetivo a tratar durante una quema prescripta. Los cambios en las métricas en el post fuego estuvieron generalmente correlacionadas con las valores iniciales de las métricasy con los cambios iniciales de los valores de esas métricas Especialmente en los estratos altos y bajos de los arbustos En los cuales los coeficientes de correlación de Pearson y Spearman estuvieron por encima de 0,400 y tan altos como 0,955. También documentamos correlaciones entre las métricas basadas en TLS y los cambios iniciales y la tasa de cambio en el post fuego por el NDVI y NBR y en el índice visual compuesto de campo (CBI). Finalmente Documentamos que las métricas a nivel de parcelas pueden agregarse para caracterizar unidades de quema completas.

Conclusiones El método multi-temporal TLS complementa las determinaciones basadas mediante el uso de NBR y CBI y mejora la cuantificación de la eficacia de las quemas prescriptas para reducir la abundancia de combustibles en el estrato de arbustos Tanto bajos como altos

Introduction

Prescribed fire treatments can be an effective means to reduce fire risk and accomplish silvicultural and cultural objectives via the controlled consumption of fuel (McCaw et al. 1996; Arkle et al. 2012; Kobziar et al. 2015; Scherer et al. 2016; Hiers et al. 2020); however, inconsistent or inadequate documentation of treatment efficacy on most landscapes has historically limited the ability to evaluate objectives, let alone adapt management decisions such as when to re-apply fire (Williams et al. 2024). Documenting the efficacy of prescribed fire treatments is often conducted using pre- and post-fire, field-based assessments at the plot-scale to estimate fuel characteristics and associated change (Lutes et al. 2006). Collecting field-based data within plots before and after a fire provides a means for land managers to characterize the amount of fuel removed. Repeat collection over time, such as once a year, can be used to characterize the rate and amount of fuel accumulation and can inform when another prescribed burn should be administered. Field-based methods often provide no information about ladder (e.g., shrubs or midstory vegetation) or canopy fuels, the quantities of which are necessary to fully characterize fire hazards and parameterize models capable of simulating prescribed fire behavior (Riccardi et al. 2007; Linn et al. 2020; Tutland et al. 2025).

As one example of a common method to characterize post-fire landscape conditions, the composite burn index (CBI) (Key and Benson 1999a, b) makes use of visual assessments to characterize the severity of a prescribed or wildfire for different forest strata: substrate, litter, and duff; herbaceous vegetation and low shrubs; tall shrubs and small trees; and overstory trees. Factors considered include the amount of litter or duff consumed, amount of subcanopy fuel consumed, crown scorch, foliage consumption, height of bole char, and overstory mortality. For each stratum, a score between 0 and 3 is assigned where 0 indicates no change post-fire, or unburned, and 3 indicates high severity (e.g., complete consumption or mortality in the stratum). The stratum-level CBIs can then be averaged to obtain a total CBI (Key and Benson 1999b).

Methods for characterizing post-fire conditions have also been developed that rely on multispectral remotely sensed data (Key and Benson 1999a; Lewis et al. 2006; Lutes et al. 2006). For example, the difference normalized burn ratio (dNBR) (Key and Benson 1999a, b) uses surface reflectance data, such as those provided by the Landsat sensors or the Sentinel-2 Multispectral Instrument (MSI), to characterize burn severity and differentiate burned areas from unburned forests or vegetation. This index is often calibrated relative to ground-based methods, such as CBI (Miller et al. 2009). In contrast to photosynthetically active vegetation, burned areas are characterized by higher shortwave infrared (SWIR) reflectance in comparison to near infrared (NIR) reflectance. Also, fire may increase the SWIR reflectance of the underlying soil, and reduced vegetation cover may increase the impact of soil characteristics on the resulting SWIR spectral measurement at the pixel location. The presence of ash and char may also increase SWIR spectral reflectance (Key and Benson 1999a, b). Despite providing data about the entire forest profile, fire effects cannot be separated by the vertical stratum in which they occurred. Expanding upon studies using a pre- and post-fire image pair to calculate dNBR, several prior studies have explored change over time using a time series of spectral measurements (e.g., Veraverbeke et al. 2010; Frazier et al. 2018; Bright et al. 2019)). As vegetation recovers and fuel materials accumulate in the subcanopy, it is expected that the NBR will increase. Other studies have used a normalized difference vegetation index (NDVI) (Eq. 3) (Rouse et al. 1973), a time series of NDVI measurements, or change in NDVI (dNDVI) to characterize vegetation changes after a fire (e.g., Goetz et al. 2006; Hope et al. 2007; Gitas et al. 2012; Veraverbeke et al. 2012)). Since NBR and NDVI provide different but complimentary information, a time series of both of these indices are explored in this study.

$$\text{Normalized burn ratio (NBR)} = \frac{\text{NIR} - \text{SWIR}}{\text{NIR} + \text{SWIR}} \tag{1}$$

$$\text{Difference normalized burn ratio (dNBR)} = \text{NBR}_{\text{pre-fire}} - \text{NBR}_{\text{post-fire}} \tag{2}$$

$$\text{Normalized difference vegetation index (NDVI)} = \frac{\text{NIR} - \text{Red}}{\text{NIR} + \text{Red}} \tag{3}$$

Airborne and terrestrial light detection and ranging (lidar) techniques have emerged as an alternative or complimentary means to characterize forest structure, fuel conditions, and post-fire change (Andersen et al. 2005; Loudermilk et al. 2007; Akay et al. 2009; Gajardo et al. 2013; Skowronski et al. 2014; Inan et al. 2017; Calders et al. 2020; Wallace et al. 2022; Murphy et al. 2024). Airborne laser scanning (ALS) methods for assessing wall-to-wall fuel conditions and treatment impacts have been available for more than two decades. Unfortunately, the economics of ALS cause the spatiotemporal scale of ALS collections to be considerably larger and longer than the spatiotemporal scale of forest treatment and evaluation, making ALS an impractical tool for treatment effects monitoring. Further, when forest overstory is present, canopy occlusion can hinder characterization of midstory or surface fuels, which are of primary concern for fuel hazard and fuel reduction treatments. Terrestrial laser scanning (TLS) only matured as a management-scale fuels monitoring approach within the past decade (Grau et al. 2017; Donager et al. 2019; Wallace et al. 2022; Murphy et al. 2024). Both ALS and TLS platforms add significant value to the characterization of fuels because of their depiction of vertical forest structure, which contrasts with the spectral reflectance and ocular estimates described above (Skowronski et al. 2020; Gallagher et al. 2021). In particular, TLS-based approaches have gained recent attention as cost effective, manager-friendly means of providing monitoring data at local-landscape scales with greater accuracy, detail, and speed than traditional field-based approaches (Murphy et al. 2024; Tenny et al. 2025; Tutland et al. 2025).

In this study, we focus on the analysis of a time series of measurements from repeated TLS scans to characterize prescribed fire efficacy at the plot- and burn-unit scales. We make use of a pre-burn scan, post-burn scan, and repeat scans for four subsequent years to characterize vegetation regrowth or fuel accumulation over time. Based on a review of existing literature and to the best of our knowledge, this is the first study that attempts to characterize long-term fuel trends using TLS, as opposed to relying on a single pair of pre- and post-fire scans. We aim to explore these data for documenting and monitoring prescribed fire efficacy and fuel characteristics, as well as to make comparisons to other commonly used burn severity assessment methods, including CBI and Sentinel-2 MSI-derived NBR/dNBR and NDVI/dNDVI data. This is a continuation and expansion of our prior study, Gallagher et al. (2021), in which we compared plot-level, TLS-derived metrics with CBI using a single pair of pre-fire and post-fire scans. The analysis of time series data presented here allows for documenting vegetation regrowth and fuel structure modification over a 4-year period. We argue that this is of practical value since this is the time frame commonly considered by land managers when determining when to re-apply prescribed fire treatment in the landscape in question: the Pine Barrens within the state of New Jersey, USA.

Background

The prediction or characterization of a variety of subcanopy attributes have been explored using TLS data, including fuel depths by stratum (Rowell et al. 2016), fuel loadings (Alonso-Rego et al. 2021; Luciano et al. 2025), average shrub heights (Alonso-Rego et al. 2020; Maxwell et al. 2023), occupied volume (Rowell et al. 2020), shrub fuel bulk density (Hudak et al. 2020), and near-surface and intermediate canopy heights (Hillman et al. 2021). TLS data collection methods and associated field sampling protocols have been developed (Pokswinski et al. 2021) and implemented by the Interagency Ecosystem LiDAR Monitoring (IntELiMon) program in the USA (https://dmsdata.cr.usgs.gov/lidar-monitoring/viewer/). To enhance practicality, there has generally been an interest in collecting data using affordable TLS units and single-position scans per field plot. This reduces field collection time, post-processing requirements, and the need to perform coregistration, which is often difficult in forested settings due to the complex point cloud structure, movement of vegetation between scans due to wind, and lack of reference surfaces (Pokswinski et al. 2021). Further, prior studies, including Bester et al. (2023) and Tenny et al. (2025), document that merging data from multiple scan positions does not generally improve plot-scale characterization.

In order to estimate parameters of interest from TLS-derived metrics, it is common to collect associated field data, with measurement approaches, such as Brown's transects or destructive harvesting of material, and use linear or machine learning regression to estimate the variable of interest using predictor variables derived from the TLS data. These TLS-derived predictor variables are often metrics that characterize point density, distribution, or vertical structure. It is also often necessary to make use of allometric equations to estimate quantities of interest, such as biomass or bulk density, from field measurements. Following this analysis of field and TLS data from a single date, researchers have often calculated the change in metrics using pre- and post-fire scans (Loudermilk et al. 2007, 2009; Pokswinski et al. 2021; Luciano et al. 2025). In short, it is important to note that adopting TLS-based methods does not remove the need for collecting ground measurements since they are required to build relationships between TLS-derived point cloud metrics and measurements of interest. However, once a relationship is established within a specific landscape, it could be used to estimate quantities of interest at locations where only TLS data are available if consistent data collection protocols are used.

Despite issues of indirect measurement of attributes of interest and occlusion, TLS data have been documented to correlate with forest structure, fuel characteristics, and fire severity (Alonso-Rego et al. 2020, 2021; Rowell et al. 2020; Loudermilk et al. 2023). Alonso-Rego et al. (2020) documented the value of single-position TLS for estimating plot-level mean shrub height and shrub cover (Alonso-Rego et al. 2020) while Alonso-Rego et al. (2021) noted its value for estimating plot-level understory fuel depth and load within pine stands (Alonso-Rego et al. 2021). Loudermilk et al. (2023) used single-position TLS and clip plot-based field measurements and obtained R^2 values between 0.61 and 0.74 for estimating understory fuel biomass and consumption in the southeastern USA. TLS measurements have also been documented to correlate with the visual-based CBI. For example, Gallagher et al. (2021) explored the prediction of stratum-level and total CBI using single-position TLS and integrated RGB camera-derived metrics where the strongest relationships were generally observed for total, tree, and shrub CBI. The researchers noted that there is a need to develop TLS-based means to calibrate satellite-based burn severity measurements as an alternative to CBI (Gallagher et al. 2021).

Despite successes of TLS-based methods, there is generally a lack of studies that make use of a time series of TLS measurements as opposed to a single pre- or post-fire scan or a pre- and post-fire scan pair. Our review of the literature found no studies focused on multi-temporal analysis of TLS data at the plot-scale and in the context of fuel characterization and/or documentation of prescribed fire efficacy. Managers suggest wide variation in the intervals of fire treatments necessary to accomplish fuel management and silvicultural objectives (e.g., ≥ 3–16 years (Peterson and Reich 2001; Warner et al. 2020); 1–14 years (Clark et al. 2015); or 1–4 years (White et al. 1991; Burton et al. 2011)). Given these uncertain and context-specific timeframes, we argue that TLS-based estimates of vegetation reduction and subsequent re-accumulation could guide management strategy by quantifying treatment efficacy, identifying a fire-return interval for prescribed fire, and helping optimize investments in fuel management.

Methods

Study area and data

The fire-prone Pinelands National Reserve (PNR) landscape is in the state of New Jersey, USA. This area is characterized by low relief and sandy, nutrient poor, acidic soils derived from sedimentary units rich in quartz sand and gravel. The specific burn unit (Fig. 1) is within Burlington County and the Wharton State Forest. The canopy is dominated by pitch pine (*Pinus rigida* Mill.) with infrequent post oaks (*Quercus stellate* Wangenh.) The midstory primarily consists of blackjack oak (*Quercus marilandica* Muenchh.), pitch pine, and post oak while the understory includes ericaceous shrubs (predominantly *Vaccinium* and *Gaylussacia* species), laurels (*Kalmia latifolia* L. and *angustifolia* Kalm.), and shrub oaks (*Quercus marilandica* Muenchh. and *ilicifolia* Wangenh.) (Lutz 1934; McCormick 1979; Givnish 1981; Ledig et al. 2013; Gallagher 2017). Prior to burning, shrubs covered < 90% of the majority of the plots. Prescribed fire treatment was applied in March of 2021 with the last prior burn, a wildfire, occurring in June of 1939. In other words, it had experienced fire exclusion for over 80 years prior to the treatment associated with this study. An example image of the site is provided in the supplemental materials as S18 while aggregated tree data by plot are provided as S19.

We collected TLS and field-based CBI data at 40 plot locations within the burn unit. We randomly selected plots with the stipulation that they were at least 400 m apart and 100 m from roads. Using a BLK360 G1 or G2 TLS unit (Leica Geosystems, Heerbrugg, Switzerland), we collected pre-burn scans between 25 February and 3 March 2021. The sensor was mounted at 2 m above ground level and surrounding vegetation was at least 1 m from the sensor. Following the prescribed fire treatment on 6 March 2021, we collected post-burn TLS scans between 15 and 22 March 2021 and CBI data within the 10 m plot radius between 22 and 26 March 2021 using the methods outlined by the Fire Effects Monitoring and Inventory (FIREMON) system (Lutes et al. 2006) that is focused on the chemical and physical changes resulting from combustion (Gallagher et al. 2021). The ability to characterize understory vegetation was limited during the winter sampling period. For this study, we make use of the shrub, overstory, and total CBI estimates. Following the initial pre- and post-fire TLS data collections,

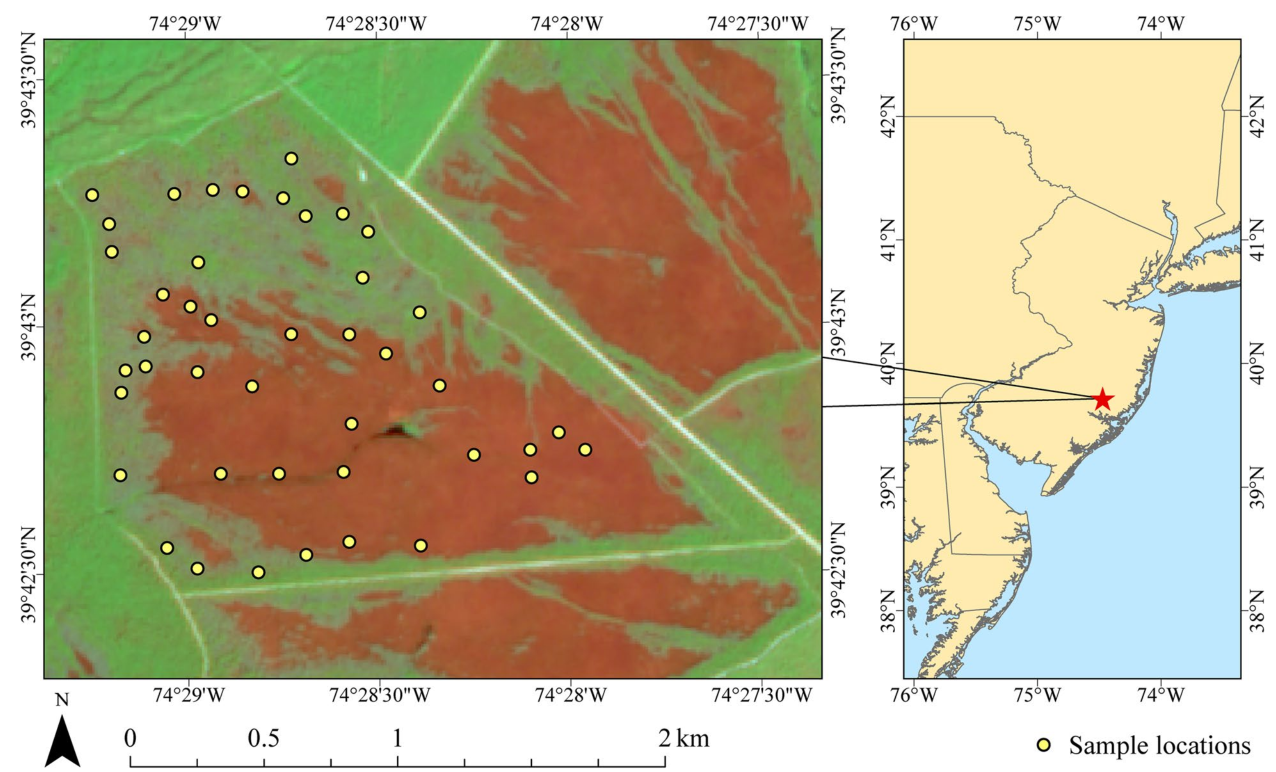

Fig. 1 Burn unit within the Wharton State Forest, Burlington County New Jersey, USA. Points represent TLS plot locations. Base imagery was collected by the Sentinel-2 Multispectral Instrument (MSI) sensor on 5 April 2021 and represents post-fire conditions. Red channel = shortwave infrared 2 (SWIR2), green channel = near infrared (NIR), and blue channel = green

we collected TLS data during the winters of 2022, 2023, 2024, and 2025, resulting in 5 post-fire scans at all 40 plot locations. We only conducted the CBI assessment after the initial fire. March is the dormant season in New Jersey and only evergreens hold leaves. Pitch pines, the dominant constituent of the overstory and mid-story, carry two cohorts of needles during the growing season, but only one between their leaf out in June and senescence around October. Nearly all understory vegetation in the shrub and herbaceous layers is without leaves at this time of year. Occurrences of evergreen sheep laurel (*Kalmia angustifolium*), mountain laurel (*Kalmia latifolia*), and inkberry holly or gallberry (*Ilex glabra*) in the understory were infrequent.

We also made use of Sentinel-2 MSI data to calculate the NBR, dNBR, NDVI, and dNDVI at a 20 m spatial resolution. A 20 m spatial resolution was used as opposed to a 10 m resolution to more closely align with the size of the field plots and to match the resolution of the SWIR band. The red and NIR channels were coarsened to a 20 m spatial resolution using pixel aggregation and the median cell value calculated from the four cells falling within the new, larger cell. Image dates are in Table 1. The pre-fire image was collected on 3 March 2021, 3 days before the prescribed fire treatment, while the post-fire image was collected on 5 April 2021. We selected images from the month of April for all subsequent post-fire data to minimize differences in phenology and illumination. We used Level-2A analysis ready data (ARD) products, which represent estimated surface reflectance and have had atmospheric correction applied.

Table 1 Dates of Sentinel-2 MSI data used to calculate NBR and dNBR

Image	Date
Pre-fire	3 March 2021
Post-fire	5 April 2021
Post-fire + 1	15 April 2022
Post-fire + 2	10 April 2023
Post-fire + 3	16 April 2024
Post-fire + 4	9 April 2025

TLS processing

Using the lidR package (Roussel et al. 2020) in the R language (R Core Team 2025), we separately processed each repeat TLS collection: a total of 240 scans. We performed ground classification and subsequent digital terrain model (DTM) calculation using a 15-m radius to circumvent edge effects in the 10-m radial plots. In order to differentiate ground and non-ground returns, we used the cloth simulation function method (Zhang et al. 2016). Conceptually, this method models the ground surface as a rigid cloth draped over an inverted point cloud, with points classified as ground returns if they intersect this surface, which has a user-specified level of rigidness (settings used in this study: class threshold = 0.1; cloth resolution = 0.1 m; rigidness = 2; time step = 0.65, maximum number of iterations = 500). After ground classification, we normalized the point cloud relative to the ground surface using the classified ground returns and a digital terrain model created at a 0.1 m spatial resolution using a *k*-nearest neighbor approach with 6 neighbors and inverse distance weighting (IDW)-based weighted averaging. Lastly, we applied a noise filter using the isolated voxels filter (IVF) method with a voxel size of 0.5 m and a maximum of 7 points.

For calculated summary metrics (Table 2), we only considered points that fell within a ring with an inner radius of 1.7 m and an outer radius of 10 m centered on the scanner location. The number of points within this ring subset varied from 3,252,850 to 5,021,238 with a mean of 4,172,133 and a median of 4,199,149 for the 240 scans analyzed in this study. The 1.7-m inner ring supported comparable summary metrics from the different scanning patterns of the Leica BLK360 G1 and G2 models used in

Table 2 Summary metrics derived from the single-position TLS measurement data for each of the six scans in the time series at all 40 plot locations. All measurements were calculated within a ring with an inner radius of 1.7 m and an outer radius of 10 m centered on the TLS sensor

Summary metric	Abbreviation	Description
Percent of not ground returns in plot radius	pNG	Percent of all returns that were not classified as ground returns
Percent of non-occluded voxels with returns (>= 0.3 & < 20 m)	pNOV Total	Percent of non-occluded voxels between 0.3 m and 20 m with associated returns; estimate of the percentage of measured volume that was occupied by vegetation
Percent of non-occluded voxels with returns (>= 5 m); canopy	pNOV Canopy	Same as pNOV Total but only considering voxels within the > 5 m and < 20 m height bin (canopy layer)
Percent of non-occluded voxels with returns (>= 2 & < 5 m); tall shrub	pNOV Tall Shrub	Same as pNOV Total but only considering voxels in the > = 2 and < 5 m height bin (tall shrub layer)
Percent of non-occluded voxels with returns (>= 0.3 & < 2 m); low shrub	pNOV Low Shrub	Same as pNOV Total but only considering voxels in the > = 0.3 and < 2 m height bin (low shrub layer)

our study. We tested the metric calculation workflow at another site where G1 and G2 scans were collected at the same location and on the same date and found that metric values were in close agreement, generally within a few percentage points. Thus, we argue that our workflow supports the comparison of data collected using the G1 and G2 models of the scanner when summary metrics are conducted at the plot scale. However, further study is necessary to explore how differences in sensor scanning patterns may impact other analyses, especially when calculating metrics for individual trees or voxels.

The first summary metric, pNG, is the percentage of returns not classified as ground measurements. As the amount of vegetation in the plot increases, the percentage of returns not classified as ground should also increase. Note that we did not incorporate any normalization to adjust for differences in return density with distance from the sensor. To characterize vegetation abundance overall or by height strata, the percentage of all returns or the count of returns per strata could be used; however, this does not take into account occlusion (Bester et al. 2023). As a result, we used alternative measures that adjust for occlusion, which were adapted from those originally reported in Bester et al. (2023). All occlusion-adjusted metrics were calculated using the full point cloud prior to any clipping, noise removal, ground classification, or ground normalization. Specifically, we considered the percentage of non-occluded voxels with returns within the 1.7 to 10 m ring and between heights of 0.3 to 20 m above the ground surface (pNOV Total) and for the 0.3 to 2 m (pNOV Low Shrub), 2 m to 5 m (pNOV Tall Shrub), and 5 m to 20 m (pNOV Canopy) height bins. We used a minimum value of 0.3 m to avoid errors or uncertainty associated with ground return classification and used a maximum height of 20 m since this was tall enough to capture all trees in the plots. Essentially, these measures offer an estimate of the percentage of the measured volume that is occupied, thereby enabling differentiation of true gaps from occlusion.

We used a multi-step process to estimate occupied volumes, true gaps, and areas of occlusion (Fig. 2). It is important to note that, since the transmission angles of all pulses with no associated returns were not recorded as part of the point cloud, this method served as a means to estimate these volumes since they could not be directly obtained from the available data. First, we converted the Cartesian coordinates to spherical coordinates with the center of the sphere aligned to the TLS sensor position (Fig. 2a). We then partitioned the extent of interest into spherical voxels covering a range of radial distances (r) and angles in the theta (θ) (azimuthal angle in the x y-plane) and phi (φ) (zenith angle) orientations using a step size of 0.5° in the θ and φ directions and a step size of 0.5 m for r (Fig. 2b). Since the sensor does not record pulses with no associated returns, we estimated the θ and φ transmission angles of these pulses, or those recorded with coordinates of [0,0,0] in the point cloud data, using a nearest neighbor-based method. A grid of regularly spaced point coordinates relative to the provided step angles of θ and φ was generated and projected onto the surface of a sphere. The actual point measurements were also projected onto the surface of the sphere, and any

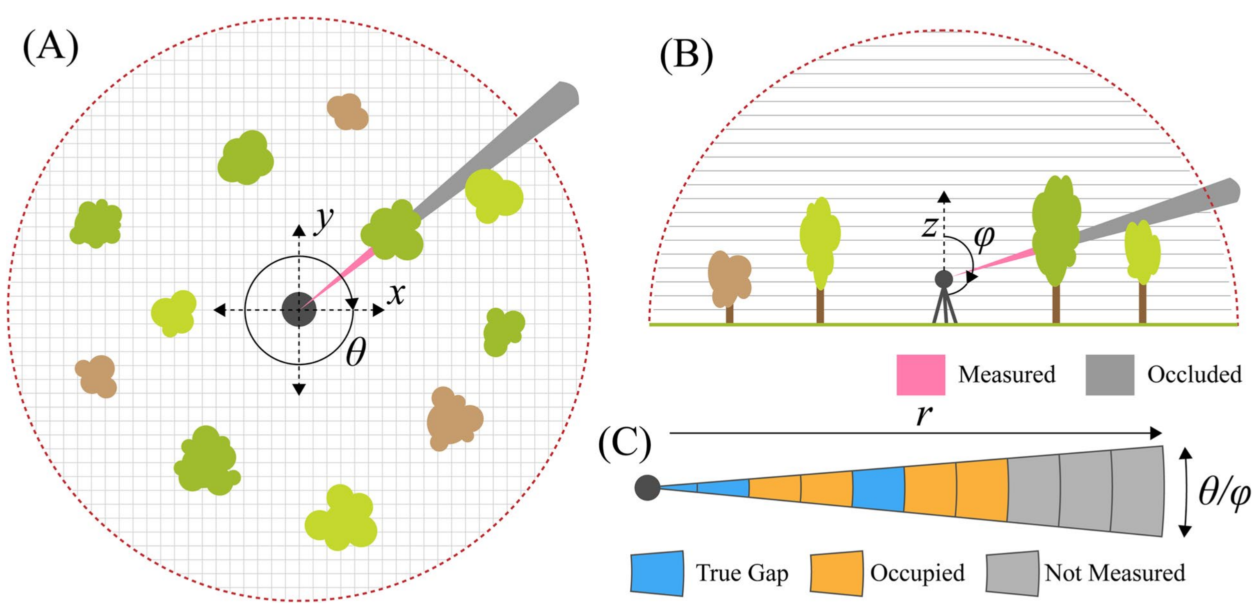

Fig. 2 Conceptualization of methods used to estimate occupied, occluded, and true gap voxels

point in the synthetic dataset that was greater than the provided step angles from any point in the actual point cloud was added to the point cloud. We next estimated the number of total pulses passing through a sequence of spherical voxels covering the same angles of θ and ϕ (Fig. 2c). Once all pulses were returned along the path, we coded all subsequent voxels as occluded. We then interpolated back to a Cartesian coordinate space and from spherical to cubic voxels with a size of 0.25 m in all three dimensions to generate summary metrics for the entire plot and for the height bins of interest. Although other summary metrics can be generated, as noted above, in this study we relied on estimates of the percentage of non-occluded voxels with returns.

Once we obtained summary metrics for each scan in the time series, we then generated a set of aggregated metrics for all 40 plots, which are listed and described in Table 3. The pre-fire metric value is derived from the TLS data collected before the prescribed fire treatment ($\mathrm{Metric}_{\mathrm{Pre}}$) while the initial change is the difference between the pre-fire metric value and its first remeasurement post-fire ($\mathrm{Metric}_{\mathrm{Pre}} - \mathrm{Metric}_{\mathrm{Post}}$). The post-fire change is the difference in the metric value between the last scan ($\mathrm{Metric}_{\mathrm{Post+4}}$) and the first post-fire scan ($\mathrm{Metric}_{\mathrm{Post}}$). The rate of post-fire change is the slope term (β_1) for a linear model in which the series of five post-fire metrics serve as the y variable and the series [0,1,2,3,4] serves as the x variable. Assuming a linear trend, the post-fire change metric represents the change in the metric value per year. Lastly, we calculated the final difference between the pre-fire scan ($\mathrm{Metric}_{\mathrm{pre}}$) and the last post-fire scan ($\mathrm{Metric}_{\mathrm{Post+4}}$). This metric is meant to characterize how post-fire conditions compare to pre-fire conditions after 4 years of fire exclusion.

In order to compare the correlation between measures, we make use of the Pearson correlation coefficient (r) (Pearson 1895), a measure of linear correlation, and the Spearman correlation coefficient (ρ) (Spearman 1987), a measure of monotonic correlation based on ranks. We use the associated t-tests to note whether the correlations are statistically significant at the 95% confidence interval (p-value = 0.05). We also compared the distribution of metric values between the pre-fire data and all post-fire collections to assess whether the metric was statistically different between the two dates using the Friedman test (Friedman 1937) followed by a pairwise Wilcoxon signed-rank test (Wilcoxon 1945) where repeat measures by site were treated as pairs. The goal of this analysis was to quantify whether the metrics had returned to pre-fire values by the year of interest, which would suggest recovery and offer evidence for the need to re-administer fire treatment.

Results

Site-level time series

Figure 3 shows the time series of pNG measurements at each plot location. The time series for the pNOV metrics are provided in the supplemental materials (S1). All plots showed reductions in pNG between the pre-fire (Pre) and first post-fire (Post) scans; however, the reduction in this metric varied. The plots in Fig. 3 have been ordered in ascending order relative to the magnitude of initial change. The amount of reduction ($\mathrm{pNG}_{\mathrm{Pre}}-\mathrm{pNG}_{\mathrm{Post}}$) varied from 6.8% (WG54) to 49.9% (WG24) with 24 plots showing a reduction greater than 25%. Similar patterns occurred on a plot-by-plot basis for the occlusion-adjusted metrics (S1); generally, the most pronounced changes were in the low shrub (pNOV Low Shrub) and tall shrub (pNOV Tall Shrub) height bins as opposed to the canopy height bin (pNOV Canopy). This is as expected since the prescribed fire treatment targeted the subcanopy fuels and canopy consumption and mortality was limited.

Following the initial change in the metrics, the general trend was recovery over the four-year period. However, similar to the initial change, the amount and rate of recovery varied by site. For pNG, the difference between Post and Post + 4 ($\mathrm{pNG}_{\mathrm{Post+4}}-\mathrm{pNG}_{\mathrm{Post}}$) varied from 2.1% (WG54) to 39.1% (WG24) and the difference between Pre and Post + 4 ($\mathrm{pNG}_{\mathrm{Pre}}-\mathrm{pNG}_{\mathrm{Post+4}}$) varied from −0.5% (WG141) to 17.2% (WG139). As with initial change, for the pNOV metrics the low and tall shrub strata generally

Table 3 Metrics derived from the time series of five measurements at each plot location

Time series metric	Description
Pre-fire metric	$\mathrm{Metric}_{\mathrm{Pre}}$
Initial change	$\mathrm{Metric}_{\mathrm{Pre}} - \mathrm{Metric}_{\mathrm{Post}}$
Post-fire change	$\mathrm{Metric}_{\mathrm{Post+4}} - \mathrm{Metric}_{\mathrm{Post}}$
Post-fire rate of change	Slope(β_1)for linear equation fit to: $x = [0,1,2,3,4]$ $y = [\mathrm{Metric}_{\mathrm{Post}}, \mathrm{Metric}_{\mathrm{Post+1}}, \mathrm{Metric}_{\mathrm{Post+2}}, \mathrm{Metric}_{\mathrm{Post+3}}, \mathrm{Metric}_{\mathrm{Post+4}}]$
Final difference	$\mathrm{Metric}_{\mathrm{Pre}} - \mathrm{Metric}_{\mathrm{Post+4}}$

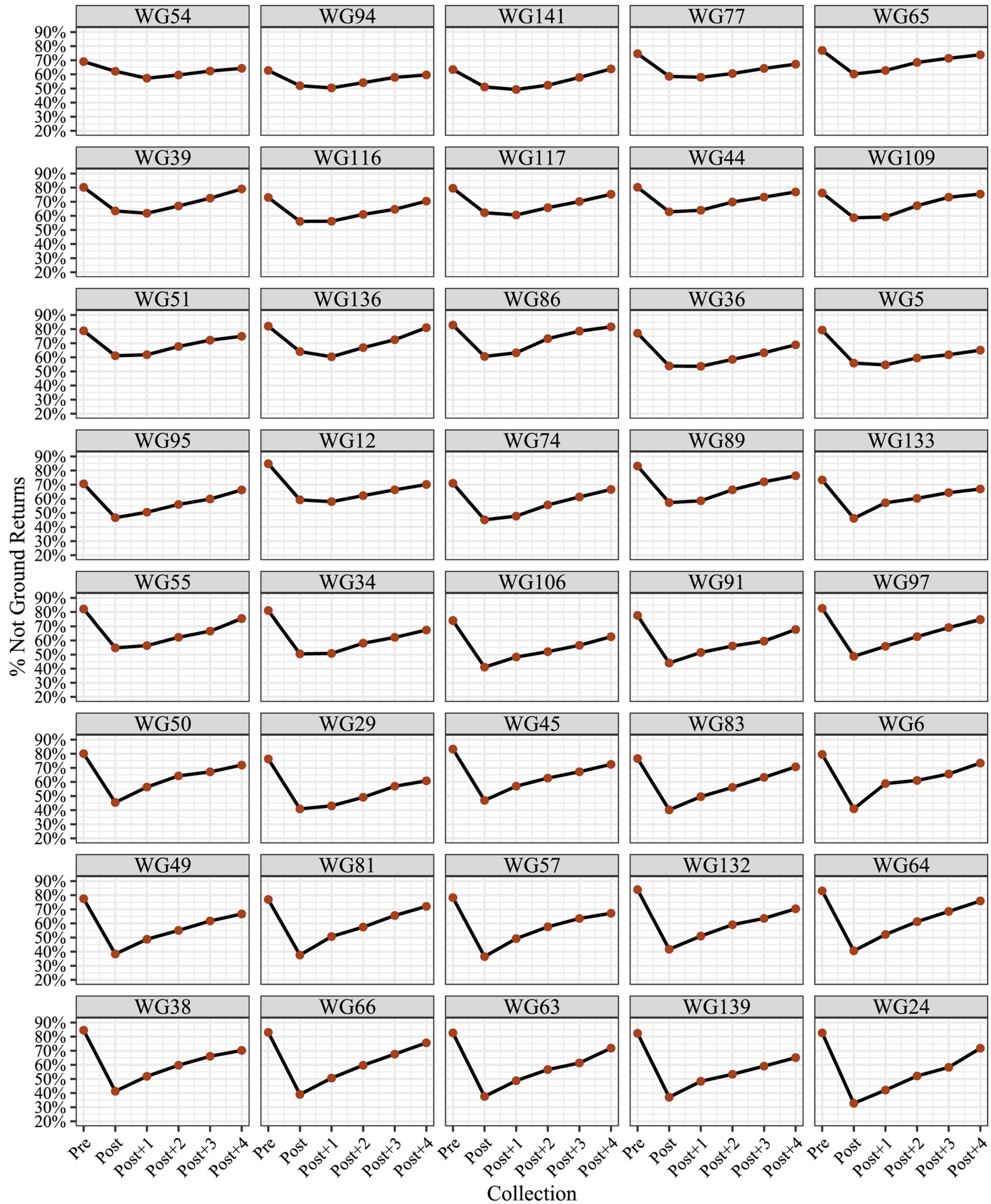

Fig. 3 Percent of all returns within the plot extent not classified as ground across all 40 sites and all six collection dates. Plots are ordered in ascending order based on the initial change in the percentage of returns in the plot not classified as ground

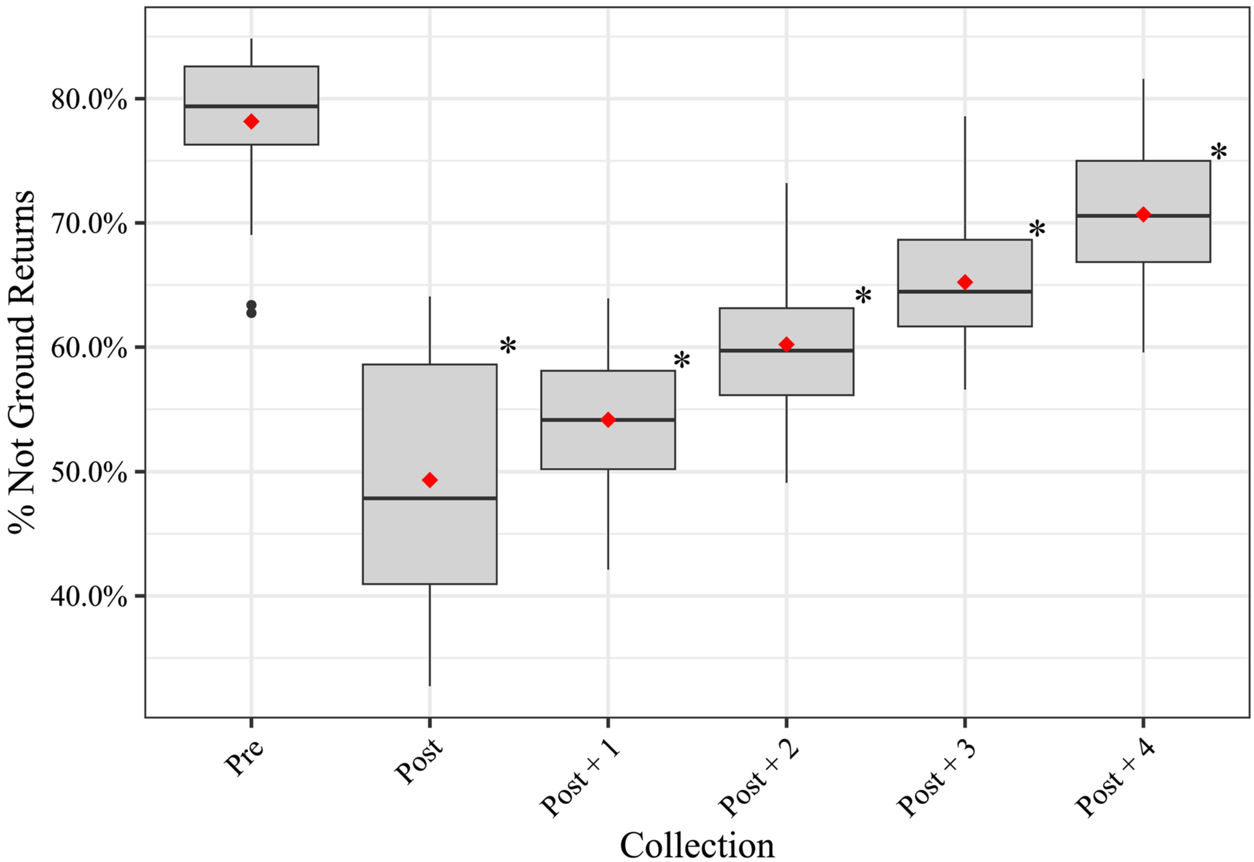

Fig. 4 Comparison of the distribution of percentage of returns from within the plot radius that were not classified as ground across 40 measured plots for all six time periods. * for post-fire collection dates indicate statistical significance at the 95% confidence interval in comparison to the pre-fire metrics. Outliers are defined as high values greater than 1.5 interquartile range (IQR) from the 3rd quartile and low values more than 1.5 IQR from the 1 st quartile. Red points represent group means

showed the greatest differences between Post and Post + 4 and Pre and Post + 4, suggesting more accumulation of materials in the subcanopy during the 4-year post-fire period in comparison to the canopy.

Some sites reached pre-fire or near pre-fire metric values by Post + 4. However, it was more common to observe lower metric values at the end of the four-year, post-fire observation period. Several sites, especially those with lower initial change values, experienced decreases in metric values for several years. This illustrates the value of longer-term monitoring and the potential to underestimate treatment effectiveness when monitoring is only conducted immediately post-burn. More analysis would be needed to determine if this can be attributed to delayed mortality.

Aggregated time series

As expected, TLS metrics declined post-fire and then recovered, as observed with the percent of returns within the plot radius not classified as ground (pNG, Fig. 4) or with the occlusion-adjusted metrics (pNOV, Fig. 5). Change was most evident for pNG and pNOV Low Shrub. This was as expected since the subcanopy fuels were the target of the treatment. Based on the observed recovery of the mean values of several metrics (e.g. pNG, pNOV Tall Shrub, and pNOV Low Shrub), the results suggest that, collectively, the site had not returned to pre-fire conditions by the end of the four-year monitoring period.

Since prescribed fire treatment decisions are commonly made at the stand- or burn unit-level, we argue that aggregated and repeat measures are valuable for land managers needing to document the efficacy of the treatment or to determine when to re-administer treatment. Table 4 provides estimates of the time required to reach pre-fire conditions for each metric using a linear equation fitted to the time series of post-fire mean metric values. Assuming a linear recovery pattern, the results suggest that pre-fire conditions in the targeted subcanopy, the low shrub and tall shrub layers, will take 9 to 10 years to recover to pre-fire metric values.

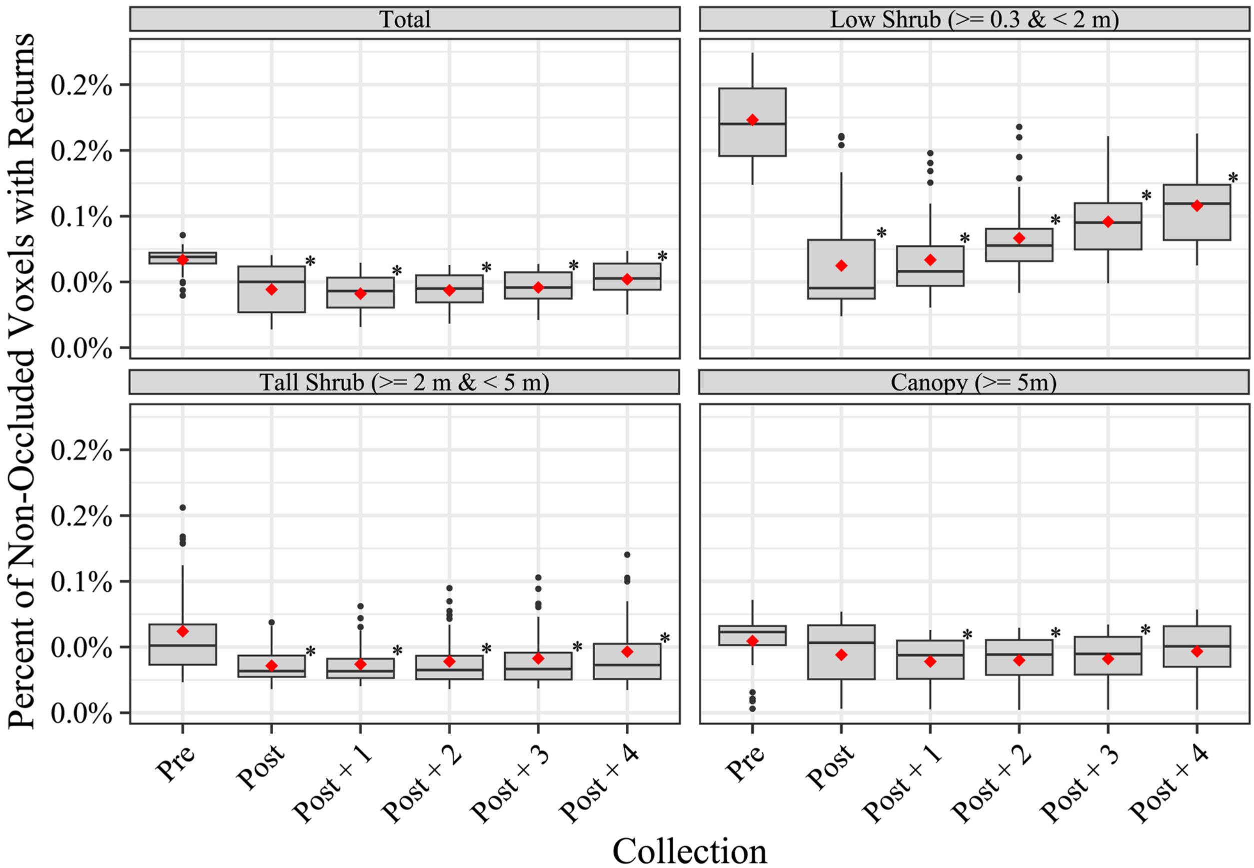

Fig. 5 Comparison of the distribution of occlusion-adjusted metrics across 40 measured plots for all six time periods. * for post-fire collection dates indicate statistical significance at the 95% confidence interval in comparison to the pre-fire metrics. Outliers are defined as high values greater than 1.5 IQR from the 3rd quartile and low values more than 1.5 IQR from the 1 st quartile. Red points represent group means

Correlations of pre-fire and post-fire metrics

Table 5 provides correlation metrics for comparing the pre-fire metric values to the change metrics. The scatterplots associated with the correlation metrics in Table 5 have been provided in the supplemental materials (S2 through S5). For initial change following treatment, the strongest relationship was observed for pNOV Tall Shrub followed by pNG and pNOV Low Shrub. For the final difference in the metric value (i.e., at the end of the study), post-fire change, and post-fire rate of change, the strongest relationships with the pre-fire metric value were all for pNOV Tall Shrub. For all comparisons, statistical significance was noted for both *r* and *ρ* at the 95% confidence interval for the pre-fire metric value and all

Table 4 Mean metric for the pre-fire scans, linear regression equation fitted to $x = [0,1,2,3,4]$ and $y = [Metric_{Post}, Metric_{Post+1}, Metric_{Post+2}, Metric_{Post+3}, Metric_{Post+4}]$ using the mean metric values, and estimate of time to recovery to pre-fire metric values using the estimated equation. t = time in years

Measure	Pre-fire mean	Equation	Estimated time to pre-fire metric value (years)
pNG	78.2%	$5.380t + 49.2$	5.4
pNOV Total	6.2%	$0.203t + 4.1$	10.3
pNOV Canopy	5.5%	$0.072t + 4.1$	19.4
pNOV Tall Shrub	6.2%	$0.258t + 3.8$	9.3
pNOV Low Shrub	17.3%	$1.202t + 5.9$	9.5
NDVI	0.368	$0.040t + 0.2$	4.2
NBR	0.273	$0.059t - 0.01$	4.8

Table 5 Correlation between pre-fire metric value and post-fire metric for all 5 measurements. Bold indicates statistical significance (*p*-value < 0.05). First value is the Pearson correlation coefficient (*r*) and the second value is the Spearman correlation coefficient (*ρ*). The associated scatterplots are provided in the supplemental materials

Pre-fire metric	Initial change	Final difference	Post-fire change	Post-fire rate of change
pNG	**0.558/0.532**	**0.441/0.413**	**0.447/0.422**	**0.496/0.456**
pNOV	0.237/**0.324**	**0.322/0.362**	0.054/0.121	0.071/0.128
pNOV Canopy	0.106/0.119	0.097/0.112	0.034/− 0.200	0.089/− 0.096
pNOV Tall Shrub	**0.955/0.847**	**0.657/0.787**	**0.747/0.569**	**0.751/0.563**
pNOV Low Shrub	**0.546/0.522**	**0.473/0.421**	**0.446/0.446**	**0.449/0.452**

Table 6 Correlation between initial metric change and all other post-fire metrics for all 5 measurements. Bold indicates statistical significance (*p*-value < 0.05). First value is the Pearson correlation coefficient (*r*) and the second value is the Spearman correlation coefficient (*ρ*). The associated scatterplots are provided in the supplemental materials

Initial change metric	Final difference	Post-fire change	Post-fire rate of change
pNG	**0.659**/0**.672**	**0.922/0.921**	**0.909/0.917**
pNOV	**0.954/0.942**	**0.877/0.856**	**0.877/0.859**
pNOV Canopy	**0.958/0.918**	**0.353/0.393**	**0.309**/0.330
pNOV Tall Shrub	**0.698/0.560**	**0.769/0.793**	**0.771/0.793**
pNOV Low Shrub	**0.674/0.680**	**0.920/0.911**	**0.912/0.898**

post-fire change metrics for pNG, pNOV Tall Shrub, and pNOV Low Shrub. Other than for the final difference metric, correlations were not statistically significant for pNOV and pNOV Canopy.

Post-fire patterns, as characterized with the TLS-based metrics, were generally correlated with the pre-fire conditions. Correlations were generally strongest for the Tall Shrub followed by the Low Shrub strata. We attribute this to the higher magnitude of change in the subcanopy since this was the target of the treatment. In contrast, correlation between pre-fire and post-fire metric summaries were generally weaker for the canopy since change in the volume of fuel material was less pronounced. Non-stratum specific metrics, pNG and pRNO Total, also generally showed weaker correlations in comparison to the subcanopy metrics, which we attribute to the integration of information across the subcanopy and canopy. This highlights the value of characterizing change at the stratum-level and especially for the stratum/strata targeted by the treatment.

Correlations of initial change and other post-fire metrics

Table 6 provides the correlation measures between the initial change in metric value and all other post-fire change metrics. The associated scatterplots have been provided in the supplemental materials as S6 through S8. Correlations between the initial metric change value and all other post-fire change metrics were generally higher than those between the pre-fire metric value and post-fire change metrics. All correlations were statistically significant. The initial change and final difference metrics were strongly correlated for all three strata (Low Shrub,

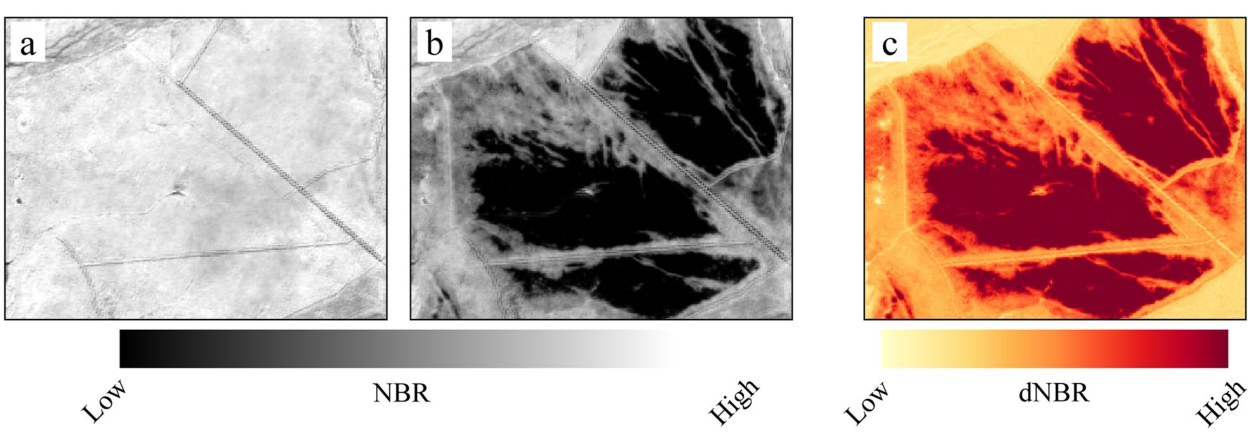

Fig. 6 NBR and dNBR results. **a** NBR calculated from pre-fire image. **b** NBR calculated from post-fire image. **c** dNBR

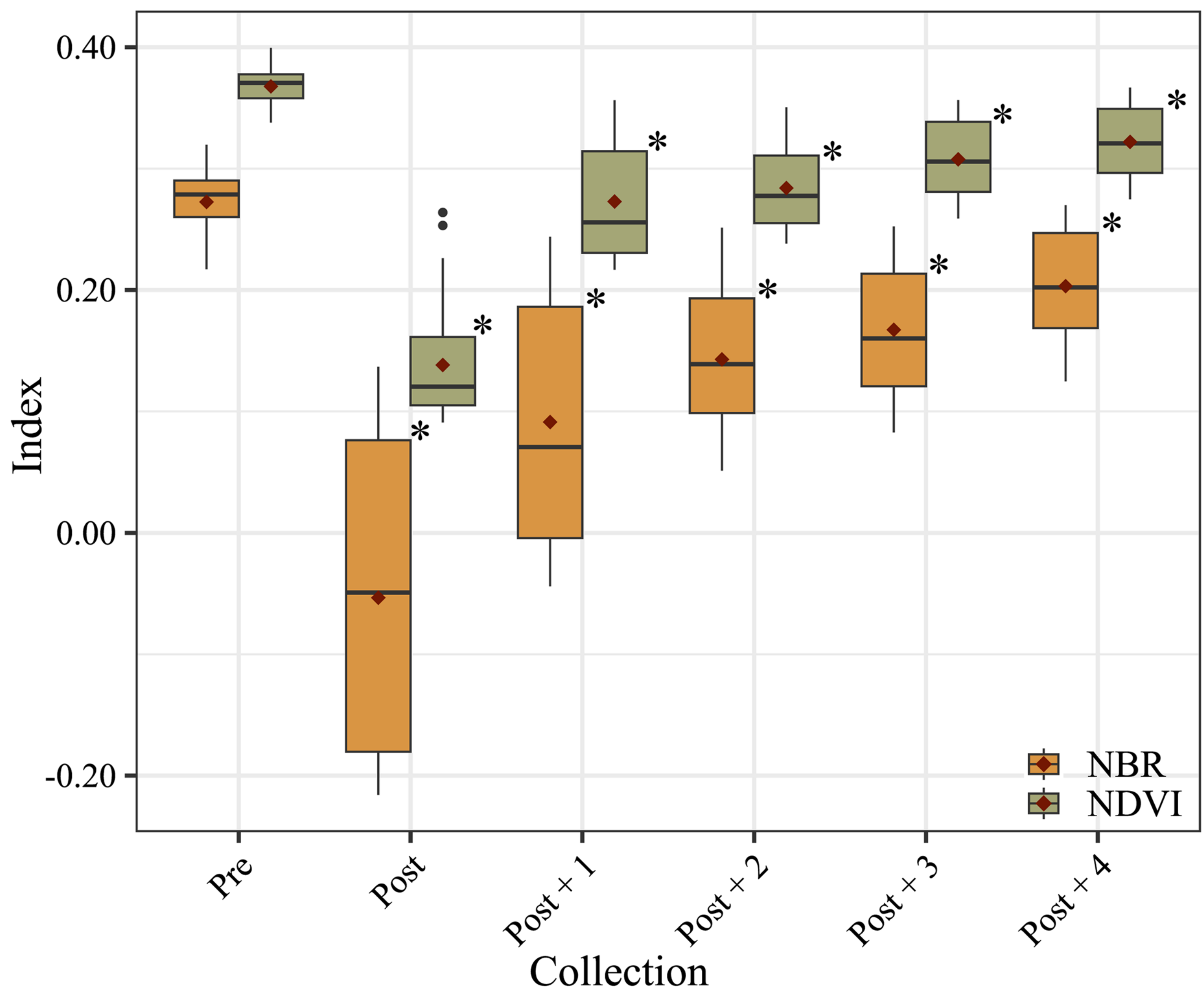

Fig. 7 Comparison of the distribution of Sentinel-2 MSI-derived NDVI and NBR across 40 measured plots for all six time periods. * for post-fire collection dates indicate statistical significance at the 95% confidence interval in comparison to the pre-fire metrics. Outliers are defined as high values greater than 1.5 interquartile range (IQR) from the 3rd quartile and low values more than 1.5 IQR from the 1 st quartile. Red points represent group means

Tall Shrub, and Canopy), and the highest correlation was for the canopy strata. The initial change had the highest correlations with post-fire change and rate of change for pNG and pNOV Low Shrub. All trends are positive, which suggests that plots with a greater initial change in the metric value tend to also experience a greater final difference after 4 years.

Comparison with NBR and NDVI

Generally, there were differences in dNBR across the burn unit immediately following the fire. Higher burn severities were reported in the southern region, which is dominated by dwarf stature pitch pines that historically burned in frequent high-intensity wildfires (Good et al. 1979). Lower burn severity was observed in the northern and northwestern region, which is dominated by typically statured pitch pines (Fig. 6).

The site-by-site time series of NDVI and NBR measurements are provided in the supplemental materials as S9 and S10 while Fig. 7 aggregates the result for each time period. Prior to the fire, NDVI and NBR values were fairly consistent across the stand, as evident by the small interquartile range (IQR). Along with reduction in NDVI and NBR following the fire, variability was also increased, which could signify variability in fire severity or treatment effects across the site. Over the recovery period, variability tended to decrease while NDVI and NBR increased, suggesting varied recovery rates by

Table 7 Correlation with dNDVI and dNBR for initial metric change for all 5 measurements. Bold indicates statistical significance (*p*-value < 0.05). First value is the Pearson correlation coefficient (*r*) and the second value is the Spearman correlation coefficient (*ρ*). The associated scatterplots are provided in the supplemental materials

Initial change metric	dNDVI	dNBR
pNG	**0.638/0.608**	**0.846/0.732**
pNOV	**0.697/0.797**	**0.882/0.853**
pNOV Canopy	**0.553/0.781**	**0.678/0.757**
pNOV Tall Shrub	**0.409/0.563**	**0.665/0.716**
pNOV Low Shrub	**0.737/0.697**	**0.824/0.807**

plot, a movement towards more homogenous foliage or vegetation conditions across the stand and re-accumulation of vegetation. As highlighted in Table 4 above, fitting a linear relationship to the post-fire NDVI or NBR observations suggests 4.2 and 4.8 years, respectively, of time before reaching pre-fire NBR conditions. However, this is assuming a linear trend while the graphs indicate recovery rates may decline or plateau. Regardless, this is notably lower than the estimated recovery time for the TLS-based metrics. This could potentially be attributed to the inadequate characterization of subcanopy fuels, or more generally the vertical re-distribution of fuels, using spectral data alone.

The correlation between TLS-based initial change metrics and dNDVI or dNBR were generally strong (Table 7). The associated scatterplots are provided in the supplemental materials as S13. At the stratum level, initial change in pNOV Low Shrub generally showed the highest correlation with dNDVI. For dNBR, the highest correlation was for pNOV followed by pNOV Low Shrub and pNG. Interestingly, pRNO Canopy generally showed lower correlations with dNDVI and dNBR than pNOV Low Shrub. This result was unexpected since NBR is likely to be most correlated with canopy changes and canopy mortality in the Pine Barrens landscape (Warner et al. 2017). This may be attributed to the limited amount of canopy change and mortality resulting from the treatment.

Table 8 provides the correlations between the post-fire rate of change of TLS-based metric values and the post fire rate of change of NDBI and NBR. The associated scatterplots are provided in the supplemental materials as S14. Similar to the initial change results, the strongest correlations for the rate of change in NDVI were for pNOV and pNOV Low Shrub. For NBR, the highest correlations were for pNOV Tall Shrub followed by pNG. The only non-statistically significant correlation was with pNOV Canopy. Generally, correlations were weaker for the rate of change results (Table 8) in comparison to the initial change results (Table 7).

Table 8 Correlation with post-fire NDVI and dNBR rate of change for post-fire rate of change for all 5 measurements. Bold indicates statistical significance (*p*-value < 0.05). First value is the Pearson correlation coefficient (*r*) and the second value is the Spearman correlation coefficient (*ρ*). The associated scatterplots are provided in the supplemental materials

Post-fire rate of change	NDVI Post-fire rate of change	NBR Post-fire rate of change
pNG	**− 0.397/ − 0.459**	**0.708/0.696**
pNOV	**− 0.643/ − 0.646**	**0.624/0.633**
pNOV Canopy	**− 0.420/ − 0.378**	0.089/0.089
pNOV Tall Shrub	**− 0.531/ − 0.515**	**0.739/0.735**
pNOV Low Shrub	**− 0.392/ − 0.508**	**0.530/0.532**

Comparison with CBI

Before discussing the correlation between the TLS-based metrics and CBI, we first explore the relationship between CBI and dNDVI or dNBR. Since CBI data were only collected after the prescribed fire treatment and alongside the Post TLS data, dNDVI and dNBR were only calculated using the pre-fire and first post-fire Sentinel-2 MSI images. As highlighted in Table 9, correlations between dNDVI and dNBR were generally higher for total CBI and overstory CBI in comparison to understory CBI. Correlation between understory CBI and dNBR were generally weaker, but still statistically significant. The stronger correlations between total CBI and overstory CBI with dNBR are expected and were previously

Table 9 Correlation between initial metric change and CBI for all 5 measurements. Bold indicates statistical significance (*p*-value < 0.05). First value is the Pearson correlation coefficient (*r*) and the second value is the Spearman correlation coefficient (*ρ*). The associated scatterplots are provided in the supplemental materials

Initial change	Total CBI	Overstory CBI	Understory CBI
pNG	**0.850/0.819**	-	-
pNOV	**0.893/0.904**	-	-
pNOV Canopy	-	**0.667/0.682**	-
pNOV Tall Shrub	-	-	**0.542/0.708**
pNOV Low Shrub	-	-	**0.664/0.734**
dNDVI	**0.800/0.800**	**0.789/0.727**	**0.623/0.657**
dNBR	**0.933/0.872**	**0.984/0.838**	**0.801/0.760**

documented at another study site within the Pine Barrens landscape by Warner et al. (2017). The scatterplots associated with these correlations are provided in the supplemental materials as S15 and S16.

In comparing the initial change for the TLS-based metrics with CBI, the strongest correlation was between total CBI and pNOV Total. In other words, the percentage of non-occluded voxels with returns, a measure sensitive to changes in volume or amount of vegetation present, was most strongly correlated with the more visual-based CBI. We attribute the lower correlation between pNOV Canopy and CBI Overstory with the limited canopy mortality. pNOV Low Shrub was generally more correlated with CBI Understory than was pNOV Tall Shrub, and the pNOV Tall Shrub patterns show evidence of nonlinearity. The scatterplots associated with the correlation metrics are provided in the supplemental materials as S17.

Discussion

TLS for evaluating prescribed fire and fuel management

We argue that the method demonstrated here is practical for guiding management strategy by quantifying treatment efficacy, identifying a fire-return interval for prescribed fire, and helping optimize investments in fuel management. Practically, the workflow requires only limited TLS preprocessing (i.e., ground classification, ground normalization, and noise removal), and using a single-scan position eliminates the need to co-register multiple scans. It is not required to perform segmentation of individual trees or shrubs, which can be error prone. Since changes are analyzed at the plot- or stratum-level, as opposed to on a voxel-by-voxel basis, it was also not necessary to standardize the orientation of the scans. We used an affordable laser scanner, the Leica BLK360, to reduce the cost of the implementation. Data collection requires less than one person-day per observation increment (e.g., pre-burn, post-burn) and is repeatable and simple to implement in the field (i.e., push of a single button). Post-processing a set of five scans at a single plot site takes less than 20 min of computational time. Aggregating data across all measured plots and grouped by sampling periods supports decision making at the burn unit-level and offers a means to characterize reduction in fuels, changes in heterogeneity across the site, and recovery trajectories.

Since analysis of a time series of TLS observations is not common in the literature, our study offers several valuable lessons for forest managers considering using TLS for documenting prescribed fire and fuel management practices. First, TLS data captured spatial and temporal variability in post-fire fuel reductions. The immediate post-burn data illustrate unit-wide fuel reduction (Figs. 3, 4, and 5). Further, incorporation of strata-specific metrics allowed for characterizing where the highest degree of change occurred (Fig. 5). We specifically document reduction in the volume of material in the Low Shrub strata, which was specifically targeted during fire treatment. General patterns in the percent of total points not classified as ground in the plot (pNG) and volume-based metrics (pNOV) were initially reduced by the prescribed fire, signifying fuel consumption, followed by increasing values in the metrics over the 4-year observation period, indicating some degree of new fuel or vegetation accumulation. The magnitude of the initial change, post-fire change, final difference from pre-fire conditions, and rate of post-fire change generally varied between sites within the unit, illustrating the ability to characterize differences in fuel consumption and recovery rate between plots. Some sites, especially those with smaller initial changes in metric values (Fig. 3) continued to experience a reduction in metric values for several years, revealing an undocumented potential to underestimate treatment effectiveness when monitoring is only conducted immediately post-burn. While this study does not allow us to confirm that this can be attributed to delayed mortality, our data still illustrate how the fire treatment increased heterogeneity in the amount of vegetation in the subcanopy (Fig. 4 and 5).

Second, TLS data document variable rates of fuel recovery or vegetation change. Data collected for 4 years post-burn identifies a unit-wide pattern of fuel regeneration. Specifically, while a small proportion of the unit recovered to or near to pre-fire fuel metric values, the majority of the unit continues to have less fuel than pretreatment. Given the trends observed in this study, this burn unit is likely to regenerate to pre-fire conditions in 9–10 years (Table 4); however, this trajectory could be affected by future environmental conditions or non-linear recovery trajectories. Certainly, variability in regeneration appears linked to the magnitude of initial change and the vegetation stratum (Table 5). The strongest correlations were noted for the tall shrub stratum where all r and ρ values were above 0.550 and as high as 0.955. In other words, plots with more fuel material generally experienced more initial post-fire change and the greatest amount of recovery over the 4-year period, especially in the subcanopy. We attribute limited canopy mortality, to the subcanopy fuels being one of the primary targets of the treatment, and to the ability of subcanopy vegetation to change more rapidly. Finally, we highlight that recovery rates were faster for more intensely burned plots even though they tended to show a larger difference from initial conditions at the end of the monitoring period, signifying that higher burn intensities can create a more durable treatment effect.

Third, our study highlights that TLS data complement dNDVI, dNBR, and CBI. Comparing multi-temporal TLS and reflectance datasets illustrates that forest recovery from fire can be complex and that dNDVI or dNBR, if used alone, may result in underestimation of treatment impacts and durability, especially in the subcanopy. The initial change and post-fire rate of change in TLS-based metrics were generally correlated with dNDVI and dNBR calculated using the pre- and first post-fire image and the rate of post-fire change in NDVI and NBR (Tables 8 and 9). Although the TLS-based metrics primarily characterize change in volume or amount of material, these measures do correlate with spectral-based vegetation and burn severity indices. These results highlight the value in having alternative means, such as multi-temporal TLS, to compliment spectral-based measurements and further characterize changes in the subcanopy.

Finally, multiple years of repeat TLS data are valuable. Several prior studies have explored the utility of single post-fire or pre- and post-fire scan pairs using a single scanning position for characterizing plot-level fuel characteristics (for example, (Bauwens et al. 2016; Alonso-Rego et al. 2020, 2021; Gallagher et al. 2021; Pokswinski et al. 2021; Maxwell et al. 2023)). We argue that this study further supports the efficacy of such methods and documents the value of repeat collection for characterizing post-fire change. TLS can offer a rapid means for site assessment that is repeatable and not greatly impacted by subjectivity or human biases (Pokswinski et al. 2021). Occlusion is one potential issue with single-position data since the entire plot is not fully characterized (Heidari Mozaffar and Varshosaz 2016; Bester et al. 2023). Thus, we argue for the use of occlusion-adjusted metrics, as implemented here, to allow for more consistent comparisons across a time series and between sites.

Limitations and research needs

A key limitation of this workflow is an inability to characterize changes in the abundance of herbaceous, litter, and duff fuels due to limited changes in volumes within these strata and error associated with the ground return classification process. It is also not possible to segment different fuel components (e.g., live vs. dead, downed woody debris, or size classes of dead fuels) or the transition of materials between fuel components. There is a need to further explore methods that allow for differentiating or classifying returns into different components (Yan et al. 2025). As noted by Abdollahi and Yebra (2023), there is a need to further investigate and develop such point cloud segmentation methods focused on fuel components. However, operationalization is currently limited by labeled training data requirements and lack of generalization across landscapes (Abdollahi and Yebra 2023). There has also been an interest in developing methods that make use of mobile laser scanning units (for example, Bauwens et al. 2016; Qi et al. 2022; Hoffrén et al. 2024; Luciano et al. 2025)).

Conclusions

This study demonstrates that TLS offers a practical, efficient, and repeatable approach for evaluating prescribed fire outcomes at the plot- and burn-unit scales. Using a simplified workflow with minimal preprocessing and a single scan position, TLS captured ecologically meaningful spatial and temporal variability in fuel reduction and re-accumulation, particularly within the tall and low shrub strata. Multi-year observations document that immediate post-burn assessments may underestimate treatment effectiveness. TLS-derived structural metrics also complement spectral indices, such as dNDVI and dNBR, and visual assessments, such as CBI, by providing critical insight into three-dimensional vegetation change. While limitations remain, particularly in characterizing near-ground fuels and transition of materials between live and dead fuel components, this work highlights the strong potential of multi-temporal TLS to aid land managers in quantifying the effectiveness of fuel reduction treatments.

Abbreviations

ALS	Aerial laser scanning
ARD	Analysis ready data
CBI	Composite burn index
dNBR	Differenced normalized burn ratio
GNSS	Global Navigation Satellite System
IntELiMon	Interagency Ecosystem LiDAR Monitoring
IQR	Interquartile range
Lidar	Light detection and ranging
MSI	Multispectral Instrument
NBR	Normalized burn ratio
PNR	Pinelands National Reserve
TLS	Terrestrial laser scanning
UAV	Unpiloted aerial vehicle

Supplementary Information

The online version contains supplementary material available at https://doi.org/10.1186/s42408-026-00498-0.

Supplementary Material 1.

Acknowledgements

We would like to thank two anonymous reviewers whose comments strengthened the work. We would also like to thank Lee Minicuci, Jacob Cook, Nicole Bendixen, and William Wall for their help in the field.

Authors' contributions

Conceptualization: A.E.M., M.R.G., N.S.S.; Data Curation: A.E.M.; M.R.G.; Formal Analysis: A.E.M.; M.R.G., S.R.S., M.C.W., B.E.M., J.A.D., A.E.; Funding Acquisition: A.E.M., M.R.G., N.S.S.; Investigation: A.E.M.; M.R.G., S.R.S., M.C.W., B.E.M., J.A.D., A.E., N.S.S.; Methodology: A.E.M., M.R.G., B.E.M., N.S.S.; Project Administration: A.E.M., M.R.G., N.S.S.; Software: A.E.M.; Resources: M.R.G., N.S.S.; Supervision: A.E.M., M.R.G., N.S.S.; Validation: A.E.M.; M.R.G., S.R.S., M.C.W., J.A.D., A.E., N.S.S.; Visualization: A.E.M., S.R.S.; Writing – Original Draft: A.E.M.; Writing – Review and Editing: A.E.M.; M.R.G., B.E.M., J.A.D., N.S.S.

Funding
Funding was provided by the United States Department of Defense Strategic Research and Development Program Project grant numbers RC-2641 and RC23-8366, and US Department of Agriculture Forest Service joint venture agreements 17-JV-11242306–113, 18-JV-11242306–075, and 24-JV-11242306–019.

Data availability
The datasets used and/or analyzed during the current study are available from the corresponding author on reasonable request.

Declarations

Ethics approval and consent to participate
Not applicable.

Consent for publication
Not applicable.

Competing interests
The authors declare no competing interests.

Author details
[1]Department of Geology and Geography, West Virginia University, Morgantown, WV 26505, USA. [2]USDA Forest Service, Northern Research Station, New Lisbon, NJ 08064, USA. [3]Fire and Aviation Management, USDA Forest Service, National Office, Washington, DC 20250, USA. [4]School of Environment and Natural Resources, Ohio State University, Columbus, OH 43210, USA. [5]Forest Fire Service, New Jersey, Department of Environmental Protection, Trenton, NJ 08609, USA.

Received: 17 December 2025 Accepted: 17 April 2026
Published online: 20 May 2026

References

Abdollahi, A., and M. Yebra. 2023. Forest fuel type classification: Review of remote sensing techniques, constraints and future trends. *Journal of Environmental Management* 342 : 118315.
Akay, A.E., H. Oğuz, I.R. Karas, and K. Aruga. 2009. Using LiDAR technology in forestry activities. *Environmental Monitoring and Assessment* 151: 117–125.
Alonso-Rego, C., S. Arellano-Pérez, C. Cabo, C. Ordoñez, J. G. Álvarez-González, R. A. Díaz-Varela, and A. D. Ruiz-González. 2020. Estimating fuel loads and structural characteristics of shrub communities by using terrestrial laser scanning. *Remote Sensing* 12 (22) : 3704.
Alonso-Rego, C., S. Arellano-Pérez, J. Guerra-Hernández, J. A. Molina-Valero, A. Martínez-Calvo, C. Pérez-Cruzado, F. Castedo-Dorado, E. González-Ferreiro, J. G. Álvarez-González, and A. D. Ruiz-González. 2021. Estimating stand and fire-related surface and canopy fuel variables in pine stands using low-density airborne and single-scan terrestrial laser scanning data. *Remote Sensing* 13 (24) : 5170.
Andersen, H.-E., R.J. McGaughey, and S.E. Reutebuch. 2005. Estimating forest canopy fuel parameters using LIDAR data. *Remote Sensing of Environment* 94 (4): 441–449.
Arkle, R.S., D.S. Pilliod, and J.L. Welty. 2012. Pattern and process of prescribed fires influence effectiveness at reducing wildfire severity in dry coniferous forests. *Forest Ecology and Management* 276: 174–184.
Bauwens, S., H. Bartholomeus, K. Calders, and P. Lejeune. 2016. Forest inventory with terrestrial LiDAR: A comparison of static and hand-held mobile laser scanning. *Forests* 7 (6): 127.
Bester, M.S., A.E. Maxwell, I. Nealey, M.R. Gallagher, N.S. Skowronski, and B.E. McNeil. 2023. Synthetic forest stands and point clouds for model selection and feature space comparison. *Remote Sensing* 15 (18): 4407.
Bright, B.C., A.T. Hudak, R.E. Kennedy, J.D. Braaten, and A. Henareh Khalyani. 2019. Examining post-fire vegetation recovery with Landsat time series analysis in three western North American forest types. *Fire Ecology* 15 (1): 8. https://doi.org/10.1186/s42408-018-0021-9.
Burton, J.A., S.W. Hallgren, S.D. Fuhlendorf, and D.M. Leslie Jr. 2011. Understory response to varying fire frequencies after 20 years of prescribed burning in an upland oak forest. *Plant Ecology* 212 (9): 1513–1525.
Calders, K., J. Adams, J. Armston, H. Bartholomeus, S. Bauwens, L. P. Bentley, J. Chave, F. M. Danson, M. Demol, M. Disney, et al. 2020. Terrestrial laser scanning in forest ecology: Expanding the horizon. *Remote Sensing of Environment* 251 : 112102.
Clark, K. L., N. Skowronski, and M. Gallagher. 2015. Fire management and carbon sequestration in pine barren forests. *Journal of Sustainable Forestry* 34 (1–2): 125–146.
Donager JJ, Sankey TT, Sankey JB, Sánchez Meador AJ, Springer AE, Bailey JD (2019) Northern Arizona Ponderosa Pine Forest Treatment Terrestrial Lidar Data. US Geol Surv USGS Data Release :490
Frazier, R. J., N. C. Coops, M. A. Wulder, T. Hermosilla, and J. C. White. 2018. Analyzing spatial and temporal variability in short-term rates of post-fire vegetation return from Landsat time series. *Remote Sensing of Environment* 205:32–45. https://doi.org/10.1016/j.rse.2017.11.007.
Friedman, M. 1937. The use of ranks to avoid the assumption of normality implicit in the analysis of variance. *Journal of the American Statistical Association* 32 (200): 675–701.
Gajardo J, García M, Riaño D (2013) Applications of airborne laser scanning in forest fuel assessment and fire prevention. In: Forestry Applications of Airborne Laser Scanning: Concepts and Case Studies. Springer, pp 439–462
Gallagher, M. R. 2017. *Monitoring fire effects in the New Jersey Pine Barrens with burn severity indices*. School of Graduate Studies: Rutgers The State University of New Jersey.
Gallagher, M. R., A. E. Maxwell, L. A. Guillén, A. Everland, E. L. Loudermilk, and N. S. Skowronski. 2021. Estimation of plot-level burn severity using terrestrial laser scanning. *Remote Sensing* 13 (20) : 4168.
Gitas, I., G. Mitri, S. Veraverbeke, and A. Polychronaki. 2012. Advances in remote sensing of post-fire vegetation recovery monitoring—A review. *Remote Sens Biomass-Princ Appl* 1:334.
Givnish, T.J. 1981. Serotiny, geography, and fire in the Pine Barrens of New Jersey. *Evolution (Lancaster, Pa.)*. https://doi.org/10.1111/j.1558-5646.1981.tb04862.x.
Goetz, S.J., G.J. Fiske, and A.G. Bunn. 2006. Using satellite time-series data sets to analyze fire disturbance and forest recovery across Canada. *Remote Sensing of Environment* 101 (3): 352–365. https://doi.org/10.1016/j.rse.2006.01.011.
Good RE, Good NF, Andresen JW (1979) The pine barren plains. Pine Barrens Ecosyst Landsc :283–295
Grau, E., S. Durrieu, R. Fournier, J.-P. Gastellu-Etchegorry, and T. Yin. 2017. Estimation of 3D vegetation density with terrestrial laser scanning data using voxels. A sensitivity analysis of influencing parameters. *Remote Sensing of Environment* 191:373–388.
Heidari Mozaffar, M., and M. Varshosaz. 2016. Optimal placement of a terrestrial laser scanner with an emphasis on reducing occlusions. *Photogrammetric Record* 31 (156): 374–393.
Hiers, J. K., J. J. O'Brien, J. M. Varner, B. W. Butler, M. Dickinson, J. Furman, M. Gallagher, D. Godwin, S. L. Goodrick, S. M. Hood, et al. 2020. Prescribed fire science: The case for a refined research agenda. *Fire Ecology* 16:1–15.
Hillman, S., L. Wallace, A. Lucieer, K. Reinke, D. Turner, and S. Jones. 2021. A comparison of terrestrial and UAS sensors for measuring fuel hazard in a dry sclerophyll forest. *International Journal of Applied Earth Observation and Geoinformation* 95 : 102261.
Hoffrén, R., M.T. Lamelas, and J. de la Riva. 2024. Evaluation of handheld mobile laser scanner systems for the definition of fuel types in structurally complex Mediterranean forest stands. *Fire* 7 (2): 59.
Hope, A., C. Tague, and R. Clark. 2007. Characterizing post-fire vegetation recovery of California chaparral using TM/ETM+ time-series data. *International Journal of Remote Sensing* 28 (6): 1339–1354.
Hudak, A. T., A. Kato, B. C. Bright, E. L. Loudermilk, C. Hawley, J. C. Restaino, R. D. Ottmar, G. A. Prata, C. Cabo, S. J. Prichard, et al. 2020. Towards spatially explicit quantification of pre-and postfire fuels and fuel consumption from traditional and point cloud measurements. *Forest Science* 66 (4): 428–442.
Inan, M., E. Bilici, and A. E. Akay. 2017. Using airborne lidar data for assessment of forest fire fuel load potential. *ISPRS Annals of the Photogrammetry, Remote Sensing and Spatial Information Sciences* 4:255–258.
Key, C., and N. Benson. 1999a. *The Normalized Burn Ratio (NBR): A Landsat TM radiometric index of burn severity*. Bozeman MT: U S Geol Surv North Rocky Mt Sci Cent.
Key CH, Benson NC (1999b) The composite burn index (CBI): field rating of burn severity. Geol Surv US

Kobziar, L.N., D. Godwin, L. Taylor, and A.C. Watts. 2015. Perspectives on trends, effectiveness, and impediments to prescribed burning in the southern US. *Forests* 6 (3): 561–580.
Ledig, F.T., J.L. Hom, and P.E. Smouse. 2013. The evolution of the New Jersey Pine Plains. *American Journal of Botany* 100 (4): 778–791.
Lewis SA, Hudak AT, Robichaud PR, Lentile LB, Morgan P, Bobbitt MJ (2006) Post-wildfire ground cover mapping by spectral unmixing of hyperspectral data. In: 11th Forest service remote sensing application conference, Salt Lake City, Utah, April24. p 2006
Linn, R. R., S. L. Goodrick, S. Brambilla, M. J. Brown, R. S. Middleton, J. J. O'Brien, and J. K. Hiers. 2020. QUIC-fire: A fast-running simulation tool for prescribed fire planning. *Environmental Modelling & Software* 125 : 104616.
Loudermilk EL, Singhania A, Fernandez JC, Hiers JK, O'Brien JJ, Cropper Jr WP, Slatton KC, Mitchell RJ (2007) Application of ground-based LIDAR for fine-scale forest fuel modeling. In: In: Butler, Bret W.; Cook, Wayne, comps. The fire environment–innovations, management, and policy; conference proceedings. 26–30 March 2007; Destin, FL. Proceedings RMRS-P-46CD. Fort Collins, CO: US Department of Agriculture, Forest Service, Rocky Mountain Research Station. CD-ROM. p. 515–523
Loudermilk, E.L., J.K. Hiers, J.J. O'Brien, R.J. Mitchell, A. Singhania, J.C. Fernandez, W.P. Cropper, and K.C. Slatton. 2009. Ground-based LIDAR: A novel approach to quantify fine-scale fuelbed characteristics. *International Journal of Wildland Fire* 18 (6): 676–685.
Loudermilk, E. L., S. Pokswinski, C. M. Hawley, A. Maxwell, M. R. Gallagher, N. S. Skowronski, A. T. Hudak, C. Hoffman, and J. K. Hiers. 2023. Terrestrial laser scan metrics predict surface vegetation biomass and consumption in a frequently burned southeastern US ecosystem. *Fire* 6 (4): 151.
Luciano, B. E. K., A. T. Hudak, J. W. Atkins, B. E. North, K. M. Brock, M. J. Campbell, S.-L. Nuria, M. B. Schlickmann, F. Mauro, S. Andres, et al. 2025. Comparing Terrestrial and Mobile Laser Scanning Approaches for Multi-Layer Fuel Load Prediction in the Western United States. *Remote Sens* 17 (16): 2757.
Lutes DC, Keane RE, Caratti JF, Key CH, Benson NC, Sutherland S, Gangi LJ (2006) FIREMON: Fire effects monitoring and inventory system. Gen Tech Rep RMRS-GTR-164 Fort Collins CO US Dep Agric For Serv Rocky Mt Res Stn 1 CD 164
Lutz HJ (1934) Ecological relations in the pitch pine plains of southern New Jersey
Maxwell, A.E., M.R. Gallagher, N. Minicuci, M.S. Bester, E.L. Loudermilk, S.M. Pokswinski, and N.S. Skowronski. 2023. Impact of reference data sampling density for estimating plot-level average shrub heights using terrestrial laser scanning data. *Fire* 6 (3): 98.
McCaw, W., J. Neal, and R. Smith. 1996. Fuel accumulation following prescribed burning in young even-aged stands of karri (*Eucalyptus diversicolor*). *Australian Forestry* 59 (4): 171–177.
McCormick J (1979) The vegetation of the New Jersey pine barrens. Pine Barrens Ecosyst Landsc :229–243
Miller, J. D., E. E. Knapp, C. H. Key, C. N. Skinner, C. J. Isbell, R. M. Creasy, and J. W. Sherlock. 2009. Calibration and validation of the relative differenced Normalized Burn Ratio (RdNBR) to three measures of fire severity in the Sierra Nevada and Klamath Mountains, California, USA. *Remote Sensing of Environment* 113 (3): 645–656.
Murphy MC, Loudermilk ELL, Pokswinski S, Williams B, Link E, Lienesch L, Douglas L, Skowronski NS, Gallagher MR, Maxwell A, others (2024) Terrestrial 3D Laser Scanning for Ecosystem and Fire Effects Monitoring. bioRxiv :2024–04
Pearson, K. 1895. VII. Note on regression and inheritance in the case of two parents. *Proceedings of the Royal Society of London* 58 (347–352): 240–242.
Peterson, D.W., and P.B. Reich. 2001. Prescribed fire in oak savanna: Fire frequency effects on stand structure and dynamics. *Ecological Applications* 11 (3): 914–927.
Pokswinski, S., M. R. Gallagher, N. S. Skowronski, E. L. Loudermilk, C. Hawley, D. Wallace, A. Everland, J. Wallace, and J. K. Hiers. 2021. A simplified and affordable approach to forest monitoring using single terrestrial laser scans and transect sampling. *MethodsX* 8 : 101484.
Qi, Y., N. C. Coops, L. D. Daniels, and C. R. Butson. 2022. Assessing the effects of burn severity on post-fire tree structures using the fused drone and mobile laser scanning point clouds. *Frontiers in Environmental Science* 10 : 949442.
R Core Team. 2025. *R: A language and environment for statistical computing*. Vienna, Austria: R Foundation for Statistical Computing.
Riccardi, C.L., S.J. Prichard, D.V. Sandberg, and R.D. Ottmar. 2007. Quantifying physical characteristics of wildland fuels using the Fuel Characteristic Classification System. *Canadian Journal of Forest Research* 37 (12): 2413–2420.
Rouse JWJr, Haas RH, Schell J, Deering D (1973) Monitoring the vernal advancement and retrogradation (green wave effect) of natural vegetation
Roussel, J.-R., D. Auty, N. C. Coops, P. Tompalski, T. R. Goodbody, A. S. Meador, J.-F. Bourdon, F. De Boissieu, and A. Achim. 2020. lidR: An R package for analysis of Airborne Laser Scanning (ALS) data. *Remote Sensing of Environment* 251 : 112061.
Rowell, E., E.L. Loudermilk, C. Seielstad, and J.J. O'Brien. 2016. Using simulated 3D surface fuelbeds and terrestrial laser scan data to develop inputs to fire behavior models. *Canadian Journal of Remote Sensing* 42 (5): 443–459.
Rowell, E., E. L. Loudermilk, C. Hawley, S. Pokswinski, C. Seielstad, Ll. Queen, J. J. O'Brien, A. T. Hudak, S. Goodrick, and J. K. Hiers. 2020. Coupling terrestrial laser scanning with 3D fuel biomass sampling for advancing wildland fuels characterization. *For Ecol Manag* 462 : 117945.
Scherer, S.S., A.W. D'Amato, C.C. Kern, B.J. Palik, and M.B. Russell. 2016. Long-term impacts of prescribed fire on stand structure, growth, mortality, and individual tree vigor in *Pinusresinosa* forests. *For Ecol Manag* 368: 7–16.
Skowronski, N.S., K.L. Clark, M. Gallagher, R.A. Birdsey, and J.L. Hom. 2014. Airborne laser scanner-assisted estimation of aboveground biomass change in a temperate oak–pine forest. *Remote Sensing of Environment* 151: 166–174.
Skowronski, N.S., M.R. Gallagher, and T.A. Warner. 2020. Decomposing the interactions between fire severity and canopy fuel structure using multi-temporal, active, and passive remote sensing approaches. *Fire* 3 (1): 7.
Spearman, C. 1987. The proof and measurement of association between two things. *American Journal of Psychology* 100 (3/4): 441–471.
Tenny JT, Sankey TT, Munson SM, Meador AJS, Goetz SJ (2025) Canopy and surface fuels measurement using terrestrial lidar single-scan approach in the Mogollon Highlands of Arizona. Int J Wildland Fire 34(7)
Tutland, N. J., A. P. Wion, C. J. May, G. C. Hutchings, H. A. Nowak, J. R. Gattiker, J. K. Hiers, R. R. Linn, S. M. Pokswinski, and E. Q. Margolis. 2025. Representing 3-dimensional fuels for physics-based fire behavior models: A general framework and case study in a type-converted post-fire shrubfield. *Fire Ecology* 21 (1): 43Th.
Veraverbeke, S., S. Lhermitte, W. W. Verstraeten, and R. Goossens. 2010. The temporal dimension of differenced Normalized Burn Ratio (dNBR) fire/burn severity studies: The case of the large 2007 Peloponnese wildfires in Greece. *Remote Sensing of Environment* 114 (11): 2548–2563. https://doi.org/10.1016/j.rse.2010.05.029.
Veraverbeke, S., I. Gitas, T. Katagis, A. Polychronaki, B. Somers, and R. Goossens. 2012. Assessing post-fire vegetation recovery using red–near infrared vegetation indices: Accounting for background and vegetation variability. *ISPRS Journal of Photogrammetry and Remote Sensing* 68:28–39.
Wallace, L., S. Hillman, B. Hally, R. Taneja, A. White, and J. McGlade. 2022. Terrestrial laser scanning: An operational tool for fuel hazard mapping? *Fire* 5 (4): 85.
Warner, T.A., N.S. Skowronski, and M.R. Gallagher. 2017. High spatial resolution burn severity mapping of the New Jersey Pine Barrens with WorldView-3 near-infrared and shortwave infrared imagery. *International Journal of Remote Sensing* 38 (2): 598–616.
Warner, T.A., N.S. Skowronski, and I. La Puma. 2020. The influence of prescribed burning and wildfire on lidar-estimated forest structure of the New Jersey Pinelands National Reserve. *International Journal of Wildland Fire* 29 (12): 1100–1108.
White DL, Waldrop TA, Jones SM (1991) Forty years of prescribed burning on the Santee fire plots: effects on understory vegetation. In: Fire and the environment: ecological and cultural perspectives. USDA, Forest Service, Southeastern Forest Experimental Station., pp 51–59
Wilcoxon, F. 1945. Individual comparisons by ranking methods. *Biometrical Bulletin* 1 (6): 80–83.

Williams, J.N., L. Quinn-Davidson, H.D. Safford, A. Grupenhoff, B.R. Middleton, J. Restaino, E. Smith, C. Adlam, and H. Rivera-Huerta. 2024. Overcoming obstacles to prescribed fire in the North American Mediterranean climate zone. *Frontiers in Ecology and the Environment* 22 (1): e2687.

Yan J, Wang J, Liu X, Qi X, Feng Y, Maeda EE, Hu T, Liu L, Su Y (2025) A connectivity-based algorithm for wood–leaf separation from terrestrial laser scanning data. Methods Ecol Evol

Zhang, W., J. Qi, P. Wan, H. Wang, D. Xie, X. Wang, and G. Yan. 2016. An easy-to-use airborne LiDAR data filtering method based on cloth simulation. *Remote Sensing* 8 (6): 501.

Publisher's Note